THE JOURNAL OF PHYSICAL CHEMISTRY A

ARTICLE

pubs.acs.org/JPCA

Charge Density Analysis of 2-Methyl-4-nitro-1-phenyl-1*H*-imidazole-5-carbonitrile: An Experimental and Theoretical Study of C≡N···C≡N Interactions

Agnieszka Paul,[†,‡] Maciej Kubicki,[*,†] Adam Kubas,[§] Christian Jelsch,[‡] Karin Fink,[§] and Claude Lecomte[*,‡]

[†]Faculty of Chemistry, Adam Mickiewicz University, Grunwaldzka 6, 60-780 Poznań, Poland

[‡]Crystallographie, Résonance Magnétique et Modelisations, CRM2, UMR UHP-CNRS 7036, Institut Jean Barriol, Nancy Université, BP 70239, 54506 Vandoeuvre-les-Nancy, France

[§]Karlsruhe Institute of Technology, Institute of Nanotechnology, Hermann-von-Helmholtz-Platz 1, 76344 Eggenstein-Leopoldshafen, Germany

Supporting Information

ABSTRACT: The experimental charge density distribution was determined for 2-methyl-4-nitro-1-phenyl-1*H*-imidazole-5-carbonitryle, using the Hansen−Coppens multipole model. Free *R* factor calculations were performed with MoPro software to find optimal restraints for a physically meaningful model. The crystal packing is determined to some extent by weak C−H···O and C−H···N hydrogen bonds but mostly by a lateral electrostatic interaction between antiparallel side-by-side C≡N groups. Electrostatic energy calculations were performed based on the experimental data and are in line with the high-level, explicitly correlated theoretical SCS-RI-MP2-F12 calculations of total energy. The molecular dipole moment and atomic charge values were compared for different experimental and theoretical models, to highlight the dependence of the electrostatic property outputs on the applied restraints. Interesting O···O contacts are also described. The results are compared with two recently investigated nitroimidazole derivatives, namely, 1-(2′-aminophenyl)-2-methyl-4-nitroimidazole and 1-phenyl-4-nitroimidazole.

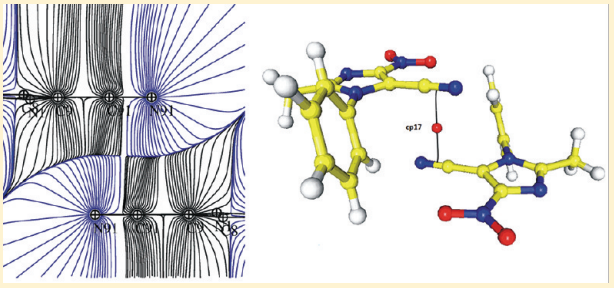

INTRODUCTION

Experimental and theoretical charge density analysis is nowadays very feasible due to the growing availability and capacity of modern diffraction instrumentation and software for such studies.[1−4] AIM (atom-in-molecules) analysis[5] based on electron density topology is the best theory to be used for analyzing and comparing experiment and DFT calculations.

Several studies were carried out to describe the electron density distribution of compounds containing a highly electronegative, pseudo-halide cyano group in different configurations and surroundings in order to shed light on the real valence structure and bonding, e.g., in small organic molecules,[6−12] metal complexes,[13,14] ionic thiocyanate compounds[15−17] or materials with NLO (nonlinear optical) properties.[18,19] A recent analysis of the Cambridge Structural Database (CSD)[20] shows the importance of dipole−dipole interactions in small-molecule crystal packing[21] and reveals that the antiparallel geometrical arrangement is dominant (57.5%) among the structures with C≡N groups while the smaller population is attributed to perpendicular (19.4%) and shared parallel (23.0%) motifs.[22] Interaction energy calculations have shown some similarities between the cyano and carbonyl group dipole−dipole interactions.[22,23] The standard resolution crystal structure analysis of 2-methyl-4-nitro-1-phenyl-1*H*-imidazole-5-carbonitrile (Figure 1), obtained from RT data[24]

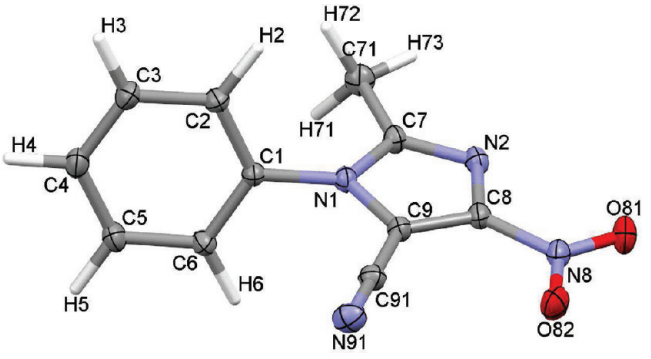

Figure 1. Anisotropic ADP ellipsoids representation of molecule **1** with atom labeling scheme. Ellipsoids are drawn at 50% probability level; hydrogen atoms are depicted as capped sticks for clarity.

revealed—beside moderate strength hydrogen bonds—the presence of the most common antiparallel C≡N···C≡N contacts.

Special Issue: Richard F. W. Bader Festschrift

Received: May 2, 2011
Revised: August 8, 2011
Published: August 30, 2011

Scheme 1

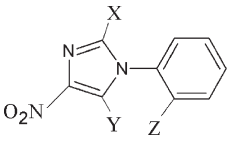

1. X = CH_3; Y = CN; Z = H
2. X = CH_3; Y = H; Z = NH_2
3. X = Y = Z = H

Here we analyze the charge density distribution in this crystal structure at 100 K (hereafter referred to as **1**), with a special emphasis on C≡N···C≡N interactions for which high level correlated SCS-RI-MP2-F12 quantum chemical calculations have also been performed.

This paper is a part of our current interests in the effect of the additional functional groups on the nitroimidazole ring in a series of 4-nitroimidazole derivatives. So far the experimental charge density distribution has been analyzed for 1-(2′-aminophenyl)-2-methyl-4-nitroimidazole[25] (hereafter referred to as **2**, cf. Scheme 1) and 1-phenyl-4-nitroimidazole[26] (hereafter referred to as **3**, cf. Scheme 1). In the present paper free *R* factor calculations were performed to obtain the most appropriate restraints for an optimal, physically meaningful model. The effect of the restraints on the charge density parameters is also discussed.

X-RAY DIFFRACTION DATA COLLECTION

A transparent-yellowish parallelepiped crystal (0.27 × 0.16 × 0.10 mm) was chosen for data collection at 100(1) K on an Oxford Diffraction SuperNova four circle diffractometer equipped with CCD detector and graphite monochromated Mo Kα radiation source (λ = 0.71073 Å). The temperature was controlled with the Oxford Instruments Cryosystem cooling device. A total of 3962 images were collected in 42 runs to achieve a high data redundancy, and 162 additional reference frames were measured to assess the stability of the crystal. Diffraction data up to sin θ/λ = 1.0 $Å^{-1}$ were collected using ω-scan method with a rotation width $\Delta\omega = 1°$. Different exposure times were chosen depending on 2θ settings of the detector: 15 s for $\theta = 0.94°$ and 30 s for $\theta = -49.29/+51.16°$, with the crystal to detector distance 55 mm. The details of the data collection and the crystallographic statistics are collected in Table 1.

The unit cell parameters were determined by least-squares fit of 49643 reflections of highest intensity. Integration of the reflection intensities, data reduction, and Lorentz-polarization corrections were done with CrysAlis Red (version 171.33.36d[27]). A numeric analytical absorption correction was applied using a multifaced crystal model,[28] and the data sorting and merging were performed with SORTAV.[29]

LEAST-SQUARES REFINEMENT

The crystal structure was solved with SIR92[30] and the independent atom model (IAM) refinement was performed with SHELXL97.[31] The crystal structure is in a good agreement with the previously published room temperature standard resolution data.[26] After the standard refinement with anisotropic model for non-hydrogen atoms and isotropic for hydrogen atoms, the SHADE server[32] was used to estimate the anisotropic thermal displacements (ADPs) of the hydrogen atoms.

The charge density distribution was subsequently refined against structure factor amplitudes with MoPro[1−3] using the multipole Hansen−Coppens model[33] for pseudoatom electron density

$$\rho_{atom}(r) = \rho_{core}(r) + P_{val}\kappa^3\rho_{val}(\kappa r) + \Sigma_l k'^3 R_l(\kappa' r)\Sigma_m P_{lm\pm}(\theta,\varphi) \quad (1)$$

where the two first terms are the spherically averaged core and valence electron densities of the atom, the last term corresponds to expansion/contraction of the nonspherical valence density in terms of real spherical harmonic functions. P_{val} is the valence population, $P_{lm\pm}$ are the multipole populations, and κ and κ' are the contraction/expansion parameters. R_l is a radial Slater

Table 1. Crystallographic Measurement and Refinement Data[a]

chemical formula	$C_{11}H_8N_4O_2$
molecular weight (g/mol)	228.20
temperature (K)	100(1)
wavelength (Å)	0.71073
crystal system	monoclinic
space group	$P2_1/n$
a (Å)	9.8484(1)
b (Å)	9.3614(1)
c (Å)	11.6487(1)
β (deg)	103.573(1)
V (Å^3)	1043.96(2)
Z	4
D_{calc} (g/cm^3)	1.452
F_{000}	472
absorption coefficient (mm^{-1})	0.11
absorption correction	analytical
T_{min}/T_{max}	0.979/0.992
crystal to detector distance (mm)	55
crystal size (mm)	0.27 × 0.16 × 0.10
sin θ/λ range (Å^{-1})	0.08−1.01
limiting indices	$-19 \le h \le 19$
	$-18 \le k \le 18$
	$-23 \le l \le 23$
reflections collected/independent	209341/8939
independent with $I > 2\sigma(I)$	6164
$R_{int}(I)$	0.066
completeness up to s = 1.00 Å^{-1}	0.9969
refinement method SPH/MULT	full matrix least-squares on F^2/F
no. of parameters SPH/MULT	186/532
weighting scheme[b]	
SPH	$w^{-1} = [\sigma^2(F_o)^2 + 0.0753P^2 + 0.0272P]$
	where $P = (F_o^2 + 2F_c^2)/3$
MULT	$w^{-1} = \sigma^2(F_o)^2$
goodness of fit on F^2 SPH/MULT	1.05/1.04
final $R(F)$ indices [$I > 2\sigma(I)$]	
SPH	R_1 = 0.044, wR_2 = 0.148
MULT R_{free}	R_1 = 0.024, wR_2 = 0.023,
MULT Free	R_1 = 0.023, wR_2 = 0.023
$\Delta\rho_{max}$, $\Delta\rho_{min}$ (e/Å^3) (sin $\theta/\lambda \le$ 1.00 Å^{-1})	
SPH	0.77(7), −0.21(7)
MULT	0.15(3), −0.14(3)

[a] SPH and MULT refer to the spherical and multipolar atom model refinement. [b] F_o means the magnitude of the F_o.

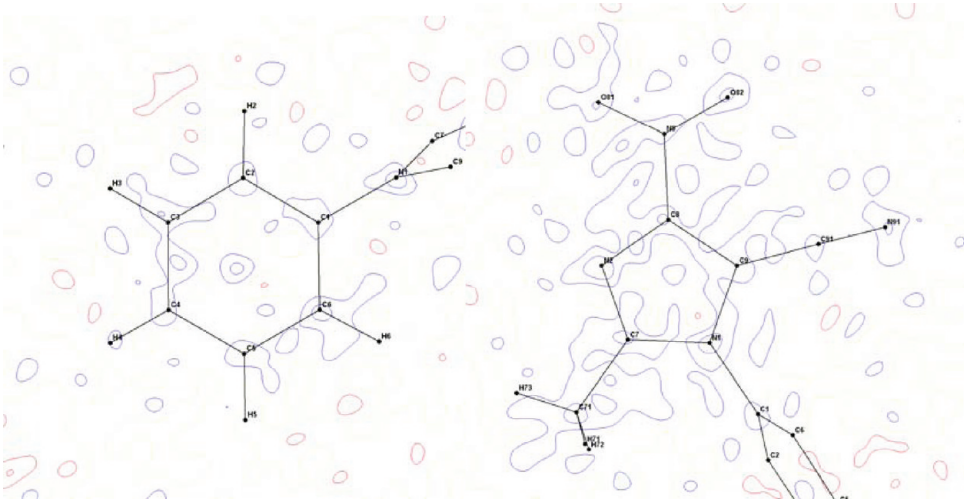

Figure 2. Residual electron density in the main planes of molecule **1**, cutoff $I > 2\sigma(I)$, resolution $s < 0.9$ Å^{-1}, contour 0.05 e/Å^3: blue, negative; red, positive.

type function

$$R_l(r) = \frac{\xi_l^{n_l+3}}{(n_l+2)!} r^{n_l} e^{-\xi_l r}, \quad nl \geq l \qquad (2)$$

The oxygen, carbon, and nitrogen atoms were refined up to octupole level ($l_{max} = 3$), except for C91 and N91 of the cyano group, for which the hexadecapole was deemed necessary due to high electron density concentration ($l_{max} = 4$) and the hydrogen atoms up to dipole level ($l_{max} = 1$). An additional investigation of the hydrogen atom modeling at the quadrupole level is currently examined, together with dipole moment calculations for different models. The n_l and ξ_l values were equal 2, 2, 2, 3, and 4.466 au^{-1} (O), 2, 2, 2, 3, (4) and 3.176 au^{-1} (C), 2, 2, 2, 3, (4) and 3.839 au^{-1} (N), and 1, 1, and 2.00 au^{-1} (H) (values in parentheses are for the hexadecapole level of carbon and nitrogen atoms). The core and valence scattering factors were calculated from Clementi and Roetti wave functions[34] and anomalous dispersion was taken into account.[35] The refinement was performed for the reflections up to $s = 1.0$ Å^{-1} with $I > 2\sigma(I)$ cutoff, which gives a satisfying number of reflections-to-parameter ratio greater than 11.

In the first step, the hydrogen atoms ADPs (HYD) were constrained to the values obtained from the SHADE server[32] and H−X distances were constrained to standard values from the neutron diffraction studies.[36] The anisotropic ADPs and the atomic positions of non-hydrogen atoms (NOH) were refined against all reflections and then against the high-resolution data only ($s > 0.65$ Å^{-1}) in IAM, to ensure proper deconvolution of the thermal motion from the deformation electron density.[33]

Subsequently, κ and κ' were set to 1.16 and 1.00, for both hydrogen and non-hydrogen atoms, respectively;[1,2] local symmetry constraints and constraints on the charge density parameters for all chemically equivalent atoms were imposed to reduce the number of variables and to produce physically meaningful parameter values. Afterward the constrained refinement of the valence and multipole populations together with the κ values was performed for all atoms until convergence. Then the ADPs and atomic positions of non-hydrogen atoms were included in the refinement. In the following steps, all the charge density similarity constrains were removed gradually. The only restraints kept until the end of the refinement were the hydrogen atoms distances ($\sigma_d = 0.01$) and the atom symmetry on N2 ($\sigma_{sym} = 0.01$), due to some diffuse static deformation density in the unrestrained model, as well as the neutrality constraint. This last multipole model—called later on the Free model—was used in R_{free} calculations,[37,38] and it appeared that the best refinement is that with weak charge density restraints on all atoms of the molecule, similar to the MoPro refinement of **2**.[25] Therefore, the last steps of the refinement were repeated with the conditions proposed in the "Free *R* factors calculations" section. The resulting refinement is called R_{free} Model.

The high quality of the refinement is validated by low values of the rigid bond test[39] (cf. Table S1, Supporting Information), with the highest values for C9−C91 equal 9×10^{-4}. The residual electron density maps for the final model R_{free} model ($R_1 = 0.024$, $R_{1free} = 0.025$, $S = 1.04$) in the main planes of the molecules show randomly distributed electron density which does not exceed ±0.15 e/Å^3 at 0.9 Å^{-1} resolution (cf. Figure 2).

FREE *R* FACTOR CALCULATIONS

Free *R* factor calculations were performed to define the optimal restraints for the charge density model, as this method allows for a cross validation using entirely diffraction data based factors. Five percent (1/20) of the reflections were used as a test set and the remaining 95% in the least-squares refinement. The strategy for *R*-free factor calculation consisted of 20 similar refinements, with the same input molecular file and the same refinement procedure. In each refinement, a different set of 5% free reflections was applied. (In the first refinement: the first, 21st reflections were free; in the second refinement, the second, 22nd reflections were free; etc.). As a result, 20 different free *R* factors (and conventional *R* factors based on 95% of the reflections) were obtained. The free *R* factors were averaged over the 20 individual free *R* factors obtained from the 20 different refinements. The refinement strategy proposed in MoPro software[2,37] was applied, with the following conditions: resolution $s < 1.0$ Å^{-1}, $I > 2\sigma(I)$, hydrogen atom distances restrained ($\sigma = 0.01$).

The analyzed factors were

$$R_1 = \sum \frac{|F_{obs} - kF_{calc}|}{\sum |F_{obs}|} \quad (3)$$

$$wR_2 = \sqrt{\frac{\sum [w(F_{obs} - kF_{calc})^2]}{\sum [w(F_{obs})^2]}} \quad (4)$$

calculated for free (5%) and working (95%) sets of reflections.

Two series of refinements were performed, at different restraints/constraints levels. (For details concerning applied restraints/constrain, see Supporting Information.)

In the first one, all κ coefficients and valence and multipole populations were constrained to be identical for the chemically equivalent atoms (e.g., C2 and C6, O81 and O82, etc.). Varying weights $w = 1/\sigma_{sym}^2$ were applied to the symmetry restraints of the atoms. For instance, *my mz* mirrors were applied on C1−C6 atoms, while C91 and N91 atoms of the nitrile group were considered to follow a cylindrical symmetry.

The quadratic function R_{sym} was added to the least-squares minimized quantity

$$R_{sym} = \sum_{i=1}^{Nat} \sum_{j} \left(\frac{P_{lm}(i,j)}{\sigma_{sym}} \right)^2 \quad (5)$$

where $P_{lm}(i,j)$ are the multipoles which do not respect the local symmetry of atom i.

By extension, a symmetry constraint can be considered as a restraint with zero tolerance, i.e., $\sigma_{sym} = 0$, meaning $w = \infty$.

As expected, the wR^2F factor decreases when the restraints weight is lowered. The wR^2F_{free} shows a U curve with a minimum observed for moderately restrained refinement ($\sigma_{sym} = 0.0125$; $wR^2F_{free} = 2.595$) (Figure 3). Increasing values of free R-factor for weak restraints at the right of Figure 3 indicates that these refinements are too loose. It is then advised to use restraints optimally weighted.

As a result, in the second series of R-free calculations, the symmetry restraints were fixed at the optimal value $\sigma_{sym} = 0.0125$ and additional refinements were performed with varying levels of restraints imposed on valence and multipole populations and κ's similarity between chemically equivalent atoms.

$$R_{sim} = \sum_{ij} \left(\frac{p_i - p_j}{\sigma_{sim}} \right)^2 \quad (6)$$

where p_i and p_j are pairs of identical parameters (κ, κ', P_{val}, P_{lm}) belonging to equivalent atoms.

Similar curves were observed as in the first refinement (Figure 4) with the minimum value for the free R factor at 2.54% ($\sigma_{sim} = 0.015$), which is lower than in the previous test series (2.59%). Therefore, the combination of the two types of restraints was chosen, based on the restraint weights bringing the lowest values of free R-factors. This final refinement strategy yields a better charge density model (R_{free} model) than the totally constrained or deconstrained refinements. However, the minimum value of wR^2F_{free} on Figure 4 is not far away from that of the totally deconstrained refinement. This indicated that the unconstrained refinement is not far from being optimal, contrary to the constrained refinement.

From now on, this optimally restrained model is used in all following experimental electron density calculations and topological analysis (R_{free} model). Applying these weak restraints

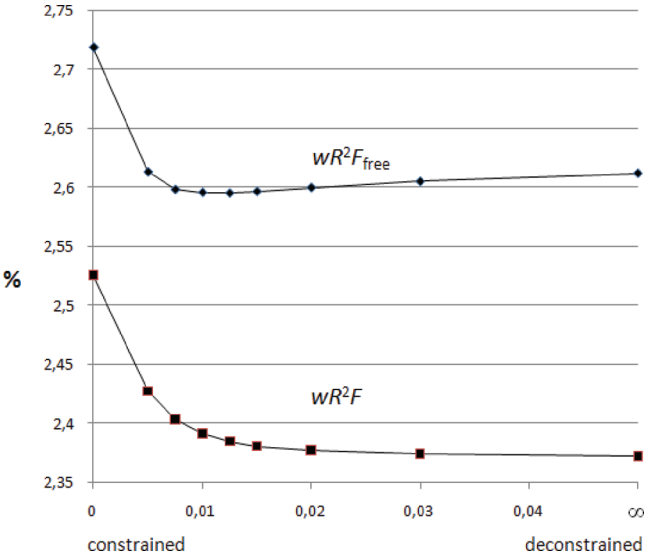

Figure 3. Crystallographic residual descriptors wR^2F and wR^2F_{free} as a function of multipole symmetry restraint sigma (σ_{sym}) for the first R-free series of tests.

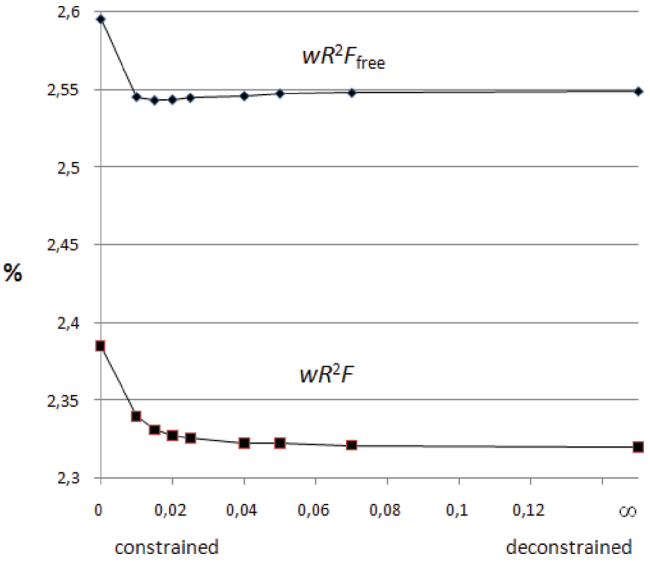

Figure 4. Crystallographic residual descriptors wR^2F and wR^2F_{free} as a function of σ_{sim} (sigma of charge density similarity restraints) for the second series of the R-free tests. The atom symmetry restraints were fixed at $\sigma_{sym} = 0.0125$.

generally did not change the values of general descriptors and accordance factors or molecular geometry, with the exception for the C≡N group (especially on the ρ_{tot} and $\nabla^2\rho$ at the critical point) and related electrostatic energy of dipole−dipole interaction (see following chapters). Therefore some outputs for the "Free" will be recalled in subsequent chapters to highlight the most significant changes. A summary of the two models used in further discussion is given in Chart 1.

ELECTRON DENSITY COMPUTATION

The deformation electron density is defined as the difference between the total molecular density described by multipolar

Chart 1

Multipolar "Free model" - derestrained, except for:

H atom distances (σ_d=0.01Å)

N2 atom symmetry σ_{sym}=0.01

electroneutrality

Multipolar "R free model" – weakly restrained charge density multipole parameters for all atoms (σ_{sym}=0.0125 σ_{sim}= 0.015)

H atom distances (σ_d=0.01Å)

electroneutrality

atom model and the superposition of spherical independent atoms (IAM, independent atom model). The experimental static deformation electron density was calculated from the crystallographic modeling as the atomic superposition sum over the molecule

$$\Delta\rho = P_{val}\kappa^3\rho_{val}(kr) - N_{val}\rho_{val}(r) + \Sigma_l\kappa'^3 R_l(\kappa' r)\Sigma_m P_{lm\pm}(\theta,\varphi) \quad (7)$$

The static and deformation maps were calculated using VMoPro and plot with MoProViewer[1−3] and the AIM charges and volumes with WinxPro (version 1.548[40]).

THEORETICAL CALCULATIONS

To gain deeper insight into the dipolar nature of the interaction between two molecules **1**, two models were set up as shown in Figure 5. Structure (a) was directly taken from the crystal structure while (b) is an acetonitrile dimer model, in which all carbon and nitrogen atoms were positioned as in the crystal while positions of the hydrogen atoms were reoptimized. The two models allowed us to study the nature and strength of the interaction between two molecules **1** as well as between an antiparallel pair of acetonitrile molecules.

We varied the distance *d* between the cyano groups between 2.3 and 12.0 Å and calculated the energy with different DFT functionals. Two popular functionals, pure Becke−Perdew 86 (BP86)[41−45] and the Becke three-parameter hybrid exchange functional combined with the Lee, Yang, and Parr (LYP) correlation functional denoted as B3LYP,[41−43,46,47] were used in connection with the triple-ζ def2-TZVPP basis set.[48,49] Since neither of these functionals account for dispersion interactions, which are expected to play an important role in dimer interactions, we decided to augment them with empirical Grimme corrections[50,51] (this is denoted as BP86+D and B3LYP+D, respectively). Moreover, the original Grimme's B97-D hybrid functional,[52] which was designed to work with these corrections, was tested. Usual counterpoise corrections (CP)[53] were added in order to correct for the BSSE (basis set superposition error). Moreover, we have taken advantage of the RI (resolution-of-identity) approximation[54,55] which significantly speeds up the calculations with a negligible error.

The two models were submitted to high-level, explicitly correlated SCS-RI-MP2-F12 calculations to benchmark our DFT results. In this treatment, the Hartree−Fock energy is corrected through first- and second-order Møller−Plesset perturbation theory (MP2).[56] In the next step, the correlation energy was calculated from explicitly correlated theory (F12 method).[57] F12 calculations converge quite quickly to the basis set limit due to additional basis functions which depend on the interelectronic distance. Moreover, the F12 method was combined with Grimme's SCS approach[58] (default scaling parameters cos = 6/5 and css = 1/3 were used) which was shown to be effective in the case of weak interactions. We used a specially optimized basis set of Peterson et al. denoted as cc-pVDZ-F12[59] with a corresponding complementary auxiliary basis (CABS).[60] Furthermore for the density fitting in the case of F12 integrals, we used large aug-cc-pwCVTZ basis sets (cbas).[61] For the density fitting of the Coulomb and exchange matrices of the Fock matrix conventional aug-cc-pVTZ basis was applied.[62] All calculations were performed with the Turbomole 6.2 program.[63]

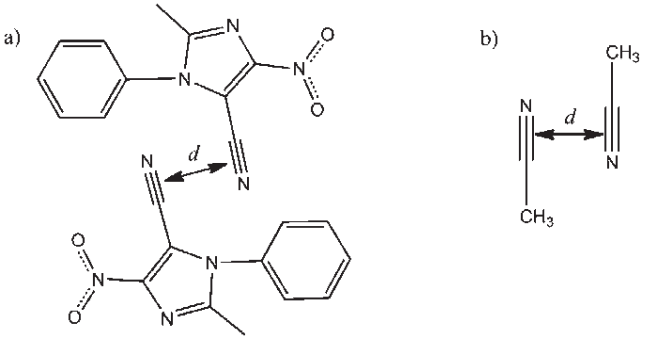

Figure 5. Two models used in quantum chemical calculations: (a) two molecules of **1** at the crystal geometry, (b) model acetonitrile dimer for pure C≡N···C≡N interaction studies.

RESULTS AND DISCUSSION

Experimental Deformation Electron Density and Topological Analysis of Covalent Bonds. The static deformation electron density drawn in the two main planes of the aromatic rings is depicted in Figure 6 (for a three-dimensional view see Figure S1 in the Supporting Information). The charge distribution in the phenyl ring is highly symmetric, as there is no additional functional group in this part of the molecule, with the

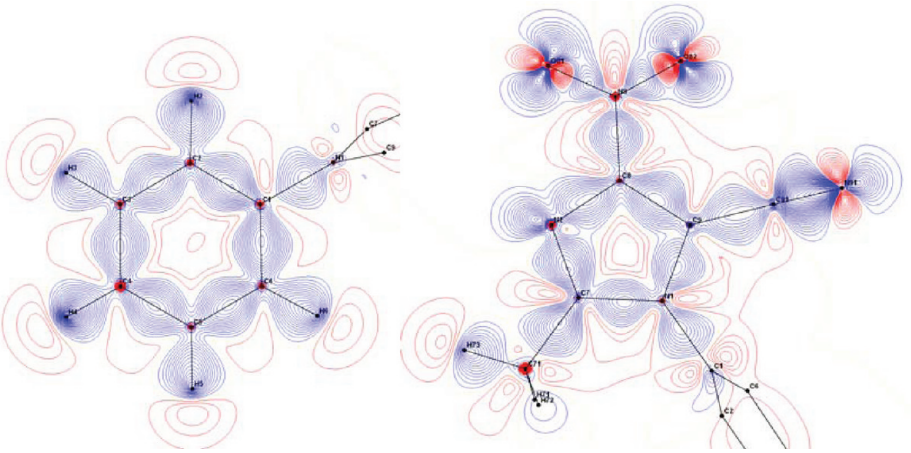

Figure 6. Static deformation density drawn in the two main planes of the molecule, contours 0.05 e/Å^3: blue, negative; red, positive.[1−3]

total electron density ρ_{cp} between 2.11 and 2.20 e/Å^3 for C−C aromatic bonds with lengths between 1.3910(4) and 1.3952(4) Å (Table S2, Supporting Information).

In the nitroimidazole part of molecule **1** (Scheme 1), the two most interesting fragments are the nitro and cyano groups. In molecule **2**, drawn in Scheme 1,[25] one of the two nitro groups had to be modeled within anharmonic approximation due to high Fourier residual peaks in the harmonic model. Despite the considerable chemical resemblance, the nitro group in **1** (N8, O81, and O82) does not show exactly the same deformation as in **2**. A reason might be the higher density of the crystal structure of **1** (1.45 g/cm^3 as compared with 1.41 g/cm^3), as well as relatively strong, directional interactions of this group with the imidazole and phenyl aromatic rings of neighboring molecule at $1 - x, -y, 2 - z$. The comparison of the parameters describing the nitro groups' bond critical points in **1** and **2**, as well as the differences between R_{free} and Free models of **1** are given in Table S4 (Supporting Information), to highlight the changes introduced by optimized restraints of the R_{free} model and to compare **1** and **2**. In general, the differences between the optimized R_{free} model and the unrestrained model are rather insignificant, except for the topological parameters of the cyano group. The total density and the Laplacian at the C≡N cp are higher in the optimal model, with differences equal 0.04 e/Å^3 (+1%) and 3.1 e/Å^5 (+12%), respectively. The ellipticity of the triple C≡N bond is nearly zero (0.01 in R_{free} and 0.00 in *Free* model), consistently with its almost cylindrical symmetry and in agreement with some published data (ε = 0.01−0.08).[8,12] The N−O distances are nearly the same (1.2245(3) and 1.2260(4) Å), while in **2**, the N−O distances within the same nitro group differ by as much as 0.005 and 0.014 Å. The values of the Laplacian and ellipticity at BCP in **1** resemble more those of the molecule modeled as anharmonic in **2**, while ρ_{tot} **1** is lower, as there is a neighboring cyano group with the highest value of the total electron density at BCP (Table S4, Supporting Information).

Electrostatic Properties. Usually, the atomic charge comparisons are not straightforward due to different definitions; therefore significant discrepancies in values and even in signs have been observed.[64,65] To emphasize and analyze some differences in atomic charges based on different definitions, Table 2 lists values of (1) $N_{val} - P_{val}$ (R_{free} model), (2) $N_{val} - P_{val}$ from the spherical-atom "kappa refinement" (multipoles = 0,[66]), (3) integrated AIM charges,[40] and (4) with Mulliken charges[67] obtained by DFT calculations (B3LYP+D). The calculations were performed for a single molecule using the conductor-like screening model (COSMO)[68] with the dielectric constant ε set to infinity to mimic the screening of the electrostatic moments in crystal.

Table 2. Atomic Charges (|e|) in Molecule 1 with Different Definitions and AIM Volumes (Å^3)

atom	MUL charge	SPH-kappa charge	AIM charge	Mulliken charge	AIM volume
C1	−0.016	−0.121	0.175	0.093	9.84
C2	−0.009	0.057	0.108	−0.220	10.85
C3	−0.055	−0.015	0.009	−0.100	12.21
C4	0.200	−0.249	0.167	−0.126	11.96
C5	−0.061	−0.017	0.066	−0.104	11.57
C6	−0.008	−0.249	−0.053	−0.216	12.43
C7	−0.194	0.287	0.720	0.218	6.59
C8	−0.067	0.062	0.623	0.080	8.48
C9	−0.265	−0.122	0.304	0.067	9.45
C71	0.236	−0.389	0.233	−0.358	9.94
C91	−0.118	0.007	0.844	−0.126	11.24
N1	−0.054	−0.025	−1.192	0.048	11.51
N2	−0.003	−0.303	−0.957	−0.269	16.54
N8	−0.073	0.532	0.189	0.499	7.92
N91	−0.097	−0.151	−1.160	−0.040	22.54
O81	−0.144	0.057	−0.390	−0.358	19.10
O82	−0.133	0.009	−0.384	−0.368	19.03
H6	0.102	0.056	0.118	0.166	5.66
H2	0.121	0.025	0.055	0.170	6.03
H3	0.162	0.160	0.156	0.156	6.70
H4	0.055	−0.014	−0.008	0.156	7.68
H5	0.157	0.019	0.120	0.157	6.04
H73	0.079	0.167	0.116	0.153	6.46
H72	0.095	0.060	0.079	0.161	5.61
H71	0.088	0.158	0.065	0.162	5.37
Σ	−0.002	0.001	0.004	0.000	260.75

As described earlier,[6,12,13] the cyano group carries a negative charge, whatever the atomic charge definition (multipolar, spherical,

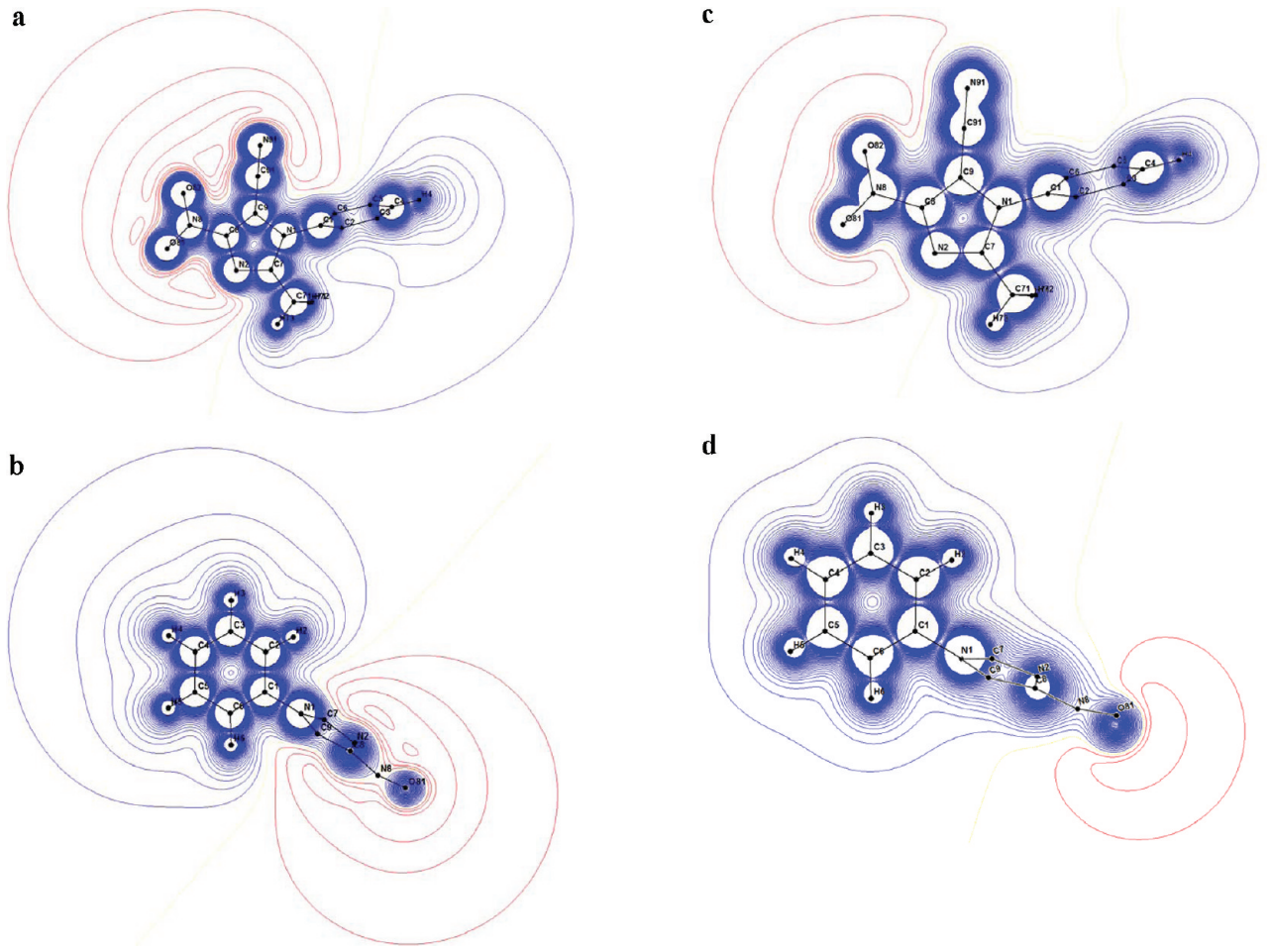

Figure 7. Total electrostatic potential drawn in the planes of the two aromatic rings: (a, b) multipolar model, (c, d) Milliken definition; contours 0.05 e/Å; blue positive, red negative.

AIM, or Mulliken) and in general the topological magnitude is much higher than the multipolar one. In **1**, the sum of charges for the C91−N91 cyano group is always negative (−0,215; −0,144, −0,316, and −0.166 |e| for the four models, respectively), but the signs and values of individual atoms vary among the definitions, with highest values for the AIM charges, as expected. On the other side, the nitro group charge (N8, O81, O82) is negative for the models MUL, AIM, and Mulliken (−0.350, −0.585, and −0.227 |e|, respectively) but positive for the kappa model (0.598 |e|). This amazing result is contrary to chemical intuition. For comparison, in the two other nitroimidazole derivatives shown in Scheme 1, the multipolar charges were equal to −0.566, −0.746 |e| in **2**[25] and −0.34 |e| in **3**[26]. The integrated AIM charges were −0.746, −0.760 |e| in (**2**) and −0.62 |e| in (**3**). Thus, despite the additional electronegative cyano group in molecule **1**, the atomic charges of **1** are closer to those in molecule **3**, in which all additional groups are replaced by hydrogen atoms.

The dipolar nature of molecule **1** is clearly seen on the electrostatic potential map for multipolar (Figure 7a,b) and Mulliken models (Figure 7c,d), with the negative area in line with the dipole moment values (Table 3). The total charge of both cyano and nitro groups is −0.9 e/Å for MUL and AIM models, but −0.52 e/Å for Mulliken definition, whereas the charge of the remaining group (phenyl ring and methyl group) carries, as expected, the opposite charges.

Table 3. Dipole Moment Values for Different Models

	B3LYP+D	B3LYP+D + COSMO	R_{free} model
μ (D)	9.68	12.47	25.71

Extensive reviews that discuss the dipole moment enhancement in molecular crystals from X-ray diffraction compared to theoretical calculations are available.[69,70] Realistic dipole moment values from multipole refinements are difficult to obtain and many factors influence the results (radial functions and flexibility, level of multipole expansion, atomic nuclear motion modeling, H atoms modeling, etc.).[69]

In molecule **1** the dipole moment calculations were performed for the optimally restrainted R_{free} model and with COSMO B3LYP+D calculations for a single molecule, respectively. As expected,[69−71] significant discrepancies occur: tracking the dipole moment changes in the refinement process in various test models showed that this parameter strongly depends on the hydrogen atoms treatement (constrained/restrained) and on the small shifts of the valence populations. A thorough study of these effects is in progress and will be discussed elsewhere.

Intermolecular Interactions. *Hydrogen Bonds.* In molecule **1**, there are three hydrogen bonds, which are however much weaker than in **2**, with donor···acceptor distances classified as moderate/weak hydrogen bonds. Molecule **1** has no "strong"

hydrogen bond donor, such as the amino group in **2**. The only possibility to form H-bonds is through H−C hydrogen atoms; cf. Table 4. The possible acceptors are the oxygen atoms of the nitro group and the nitrogen atoms of the imidazole ring and cyano group. The cyano group was reported already as a proton acceptor in H-bonds, which can successfully compete even with the amino group.[72,73]

In the room temperature crystal structure of molecule **1**,[26] only one weak hydrogen bond was taken into account in the description of the crystal packing. For the diffraction data collected at 100 K, the intermolecular contacts are shorter by about 0.1 Å (Table 4) and the number of directional contacts (D···A ≤ 3.5 Å) increases.

These hydrogen bonds and the bond critical point distances along their topological bond paths were tested by means of topological analysis and Koch and Popelier (KP) criteria described in detail in ref 74. Only two contacts (cp1 and cp3) meet the van der Waals distances condition for H-bonds; however the negative sum ($\Delta r_H + \Delta r_A$) for cp2 (Table 5) is very small and may be discussed according to the refinement strategy. (For the Free model the sum of radius differences for cp2 is slightly positive (0.051 Å).)

We also notice that the topology of the intermolecular contact at the cp17 critical point obtained with the two models show a change of ρ_{tot} (0.060−0.055 e/Å^3) and of λ_3 0(0.93−0.88 e/Å^5) for the unrestrained and R_{free}, models, respectively. These differences are inside the error bars.

Antiparallel C≡N···C≡N Interaction. As mentioned above, one of the most interesting interactions observed in this crystal structure is the antiparallel, electrostatic in nature, C≡N···C≡N interaction, which can be energetically comparable with a moderately strong hydrogen bond.[22] In the crystal structure of molecule **1**, pairs of molecules related by a crystallographic inversion center are separated by 3.22 Å (perpendicular distance between CN groups). The centrosymmetric topology of the dipole−dipole contact clearly depicts the electrostatic nature of this contact, as the bond path with its critical point (cp 17, Table S6, Supporting Information) links the triple bonds rather than the nucleus positions (Figures 8 and 10). The antiparallel arrangement of the cyano groups follows the electrostatic rules. The static deformation density in the plane of these two dipoles is depicted in Figure 9. The almost purely electrostatic nature of this interaction results in an insignificant deformation density overlap (0.0025 e/Å^3), which does not change the C≡N ellipticity ($\varepsilon = 0$). The electrostatic energy calculated with VMoPro[1−3] for a dimer composed of molecules at x, y, z and $-x+2, -y, -z+2$ is equal −19.3 kcal/mol (see following chapter).

The benchmark calculations for the interaction energy at the crystal geometry with a C≡N···C≡N distance of 3.22 Å, calculated at SCS-RI-MP2-F12 level of theory yielded −13.06 kcal/mol (see Table 5). This value differs from the experimentally obtained one (−19.3 kcal/mol) because it takes into account all types of interactions along with repulsion forces. The one-dimensional potential energy curves for the interaction of two units of molecule **1** (Figure 5a) calculated at DFT level are shown in Figure 10. The dispersion corrected functionals BP86+D and B3LYP+D show a minimum in the potential energy curve at the distance observed in the crystal. The interaction energies calculated with these functionals are −11.89 and −13.40 kcal/mol, respectively. The functional B97-D gave a

Table 4. Hydrogen Bond Geometry: Distance (Å) and Angle (deg)

	D—H···A	D—H	H···A	D···A	D—H···A
1	C2—H2···O81[a]	1.069	2.456	3.4203(4)	149.6
2	C5—H5···N2[b]	1.066	2.556	3.4911(4)	146.0
3	C6—H6···N91[c]	1.078	2.539	3.5018(4)	148.3

[a] Symmetry code: $-x+1, -y, -z+2$. [b] Symmetry code: $x+1/2, -y+1/2, z-1/2$. [c] Symmetry code: $-x+2, -y, -z+2$.

Table 5. Mutual Penetrations (Å) of the Hydrogen-Acceptor Atoms

	Δr_H	Δr_A	$\Delta r_H + \Delta r_A$
cp1	0.047	−0.005	0.042
cp2	0.031	−0.039	−0.008
cp3	0.046	−0.029	0.017
cp4	−0.050	−0.061	−0.111
cp5	−0.185	0.001	−0.184
cp6	−0.227	−0.033	−0.260
cp7	−0.234	−0.063	−0.297
cp8	−0.182	−0.167	−0.349
cp9	−0.318	−0.184	−0.502

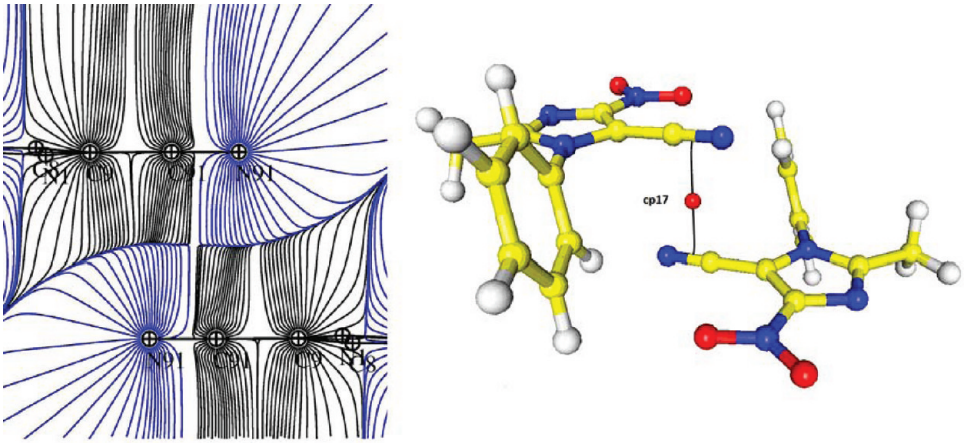

Figure 8. C≡N···C≡N interaction: (a) gradient lines in the C≡N··· C≡N plane; (b) bond path and associated critical point (cp18).

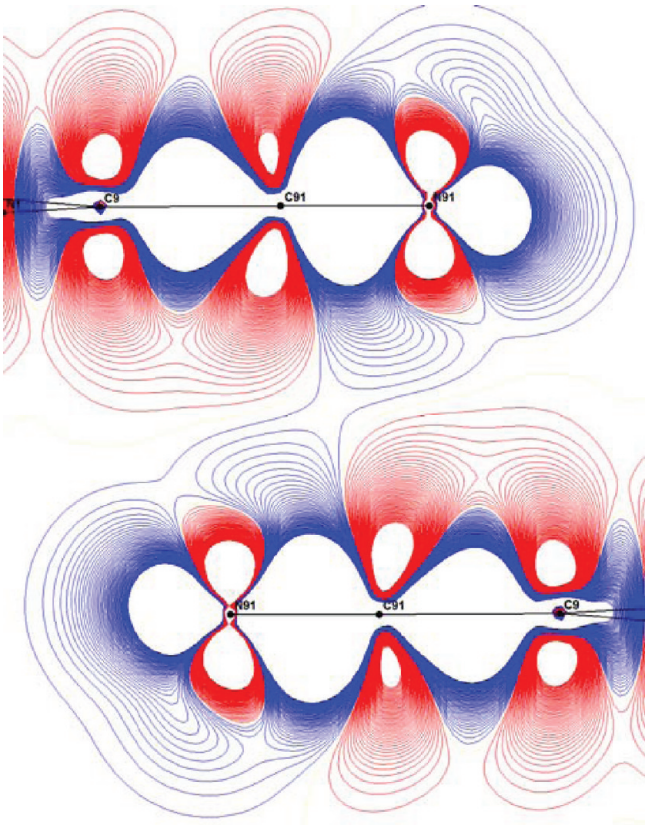

Figure 9. Deformation density around the crystallographic inversion center at the C≡N···C≡N antiparallel interaction, contours ±0.0025 e/Å^3: blue, negative; red, positive.

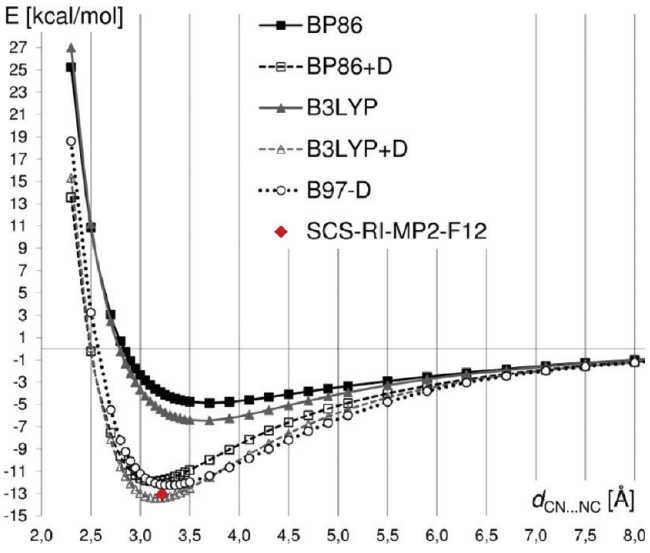

Figure 10. Energy change upon variation of C≡N···C≡N distance d between two units of molecule **1** (for the definition see Figure 5a). Different density functionals are compared to the binding energy obtained at SCS-RI-MP2-F12 level of theory.

somewhat elongated minimum distance of 3.30 Å with an interaction energy of −12.25 kcal/mol (−12.06 kcal/mol at the crystal distance). The interaction curves (Figure 10) clearly indicate that the augmentation with empirical corrections for van

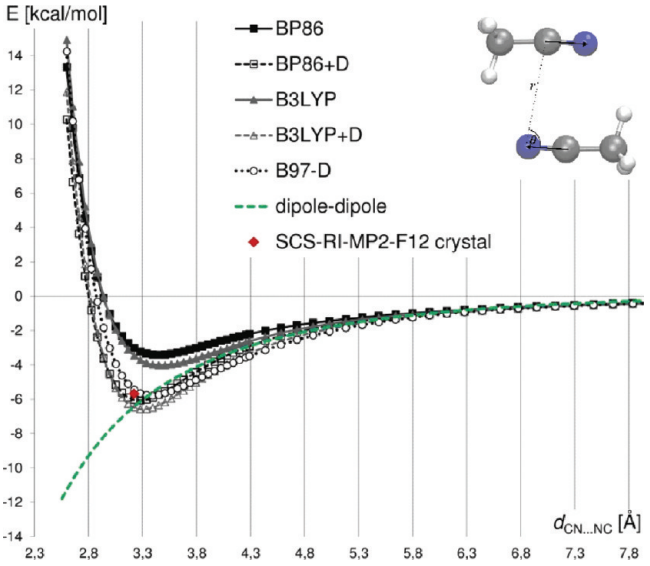

Figure 11. Energy changes upon variation of the C≡N···C≡N distance d between two acetonitrile molecules (for definition see Figure 5b). Modeled dipole−dipole interaction with dipole moments taken from B3LYP+D calculations is depicted with a green dashed curve while red point denotes the SCS-RI-MP2-F12 energy at crystal distance (3.22 Å).

Table 6. Total Interaction Energies (in kcal/mol) for a Dimer of 1 (a) and Acetonitrile Model (b), As Depicted in Figure 5. [a]

model	BP86	B3LYP	BP86+D	B3LYP+D	B97-D	SCS-RI-MP2-F12
5a	−3.89	−5.44	−11.84	−13.39	−12.18	−13.06
5b	−3.02	−3.46	−6.04	−6.48	−5.45	−5.68

[a] The calculation was done with a distance d = 3.22 Å between the two C≡N lines corresponding to the crystal structure.

der Waals interactions is crucial for the proper description of the system under consideration. Moreover, we found that two widely used functionals, BP86 and B3LYP, when corrected for dispersion are robust tools for predicting the interaction energies of weakly bound dimers, which was also the case for much larger systems (over 100 atoms) containing [2.2]paracyclophane moieties and transition metal atoms.[75]

The crystallographic study shows that the C≡N···C≡N close contact is one of the most important motifs determining the crystal packing of **1**. In order to have a closer look on this interaction, we performed a similar nonrelaxed potential energy scan involving a model acetonitrile structure depicted in Figure 5b. The resulting curves are presented in Figure 11 along with SCS-RI-MP2-F12 single-point results for equilibrium geometry (ΔE = −5.80 kcal/mol at d = 3.26 Å) and the distance found in the crystal (ΔE = −5.50 kcal/mol at d = 3.22 Å). Over 40% of the interaction energy between two units of molecule **1** comes therefore purely from the interaction of the cyano groups. All DFT+D functionals gave a bit longer C≡N···C≡N equilibrium distance than that found in the crystal structure (d = 3.37 Å for B97-D and d = 3.28 Å in the cases of BP86+D and B3LYP+D) while uncorrected BP86 and B3LYP with d = 3.45 Å are far away from the experimental value. According to Table 6, the BP89+D interaction energy at the crystal distance (−5.45 kcal/mol) is close to the one obtained with SCS-RI-MP2-F12. Similar

accuracy was observed in the case of B97-D (−5.45 kcal/mol), but unexpectedly, the B3LYP+D value (−6.48 kcal/mol) had an absolute error of 12%. The above results can be directly compared with IMPT (intermolecular perturbation theory) results of Wood et al.[22] Their value for antiparallel, coplanar C≡N···C≡N equilibrium interaction between two acetonitrile molecules was significantly smaller (−3.87 kcal/mol) than our SCS-RI-MP2-F12 value for such an interaction (−5.68 kcal/mol). However, it is well-known that the MP2 method alone (without SCS approach) purely describes weak interactions.[76] This, in connection with the small basis set used (6-31G**), leads to large errors. (Further confirmation was obtained by calculation of interaction energies at CCSD-F12/cc-pVTZ-F12 and CCSD(T)/aug-cc-pVTZ level of theory. Obtained values are −5.71 and −5.99 kcal/mol, respectively.).

In order to model the dipole−dipole interaction in an antiparallel cyano groups arrangement, we have applied the following formula to obtain the attraction energy between two antiparallel, coplanar dipoles[77]

$$E = \frac{\mu^2(3\cos^2\Theta - 1)}{4\pi\varepsilon_0 r^2} \quad (8)$$

Geometrical parameters r and θ are defined in Figure 11, and ε_0 is the dielectric constant of vacuum (8.85×10^{-12} $C^2 \cdot N^{-1} \cdot m^{-2}$). The dipole moment of the acetonitrile molecule, denoted as μ, was taken from B3LYP+D calculations. Its value (4.0 D) is close to the experimental data obtained for gas phase acetonitrile molecules (3.9 D).[78] The green dashed line in Figure 11 presents the obtained curve. The behavior of the energy decay with increasing distance d for acetonitrile molecules has an $1/d^3$ dependence in agreement with the $1/r^3$ dependence in the case of two pure electrostatic dipoles. Moreover, two interacting dipoles provide a good model for this system up to the energy minimum where the repulsion forces start to play a crucial role. Further confirmation of the purely electrostatic nature of C≡N···C≡N interaction was acquired by inspection of canonical molecular orbitals at the crystal distance (Figure 12). A linear combination of four π orbitals of individual acetonitrile molecules forms four molecular orbitals with two bonding among them (19, 20). Only MO 20 shows a small overlap between π orbitals of different molecules while the rest conserves a singular, monomolecular character. This overlap is very much in line with the observed experimental static density of cp17, as discussed above (Figure 9).

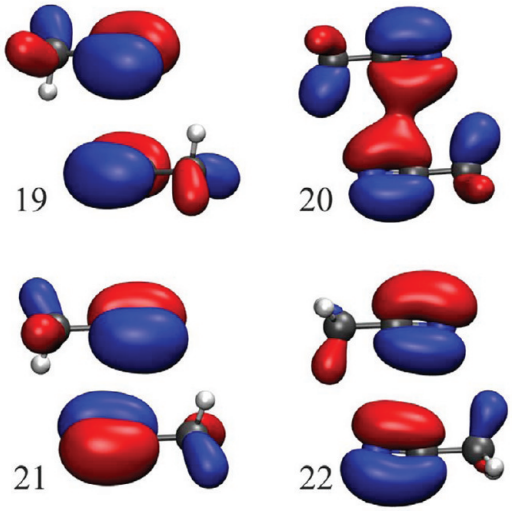

Figure 12. Images of the highest four occupied molecular orbitals obtained with the B3LYP functional (0.04 cutoff).

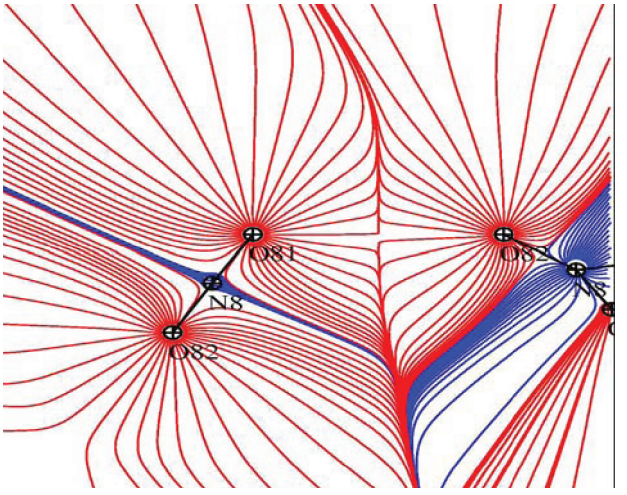

Figure 14. Representation of the gradient lines of the total electron density.

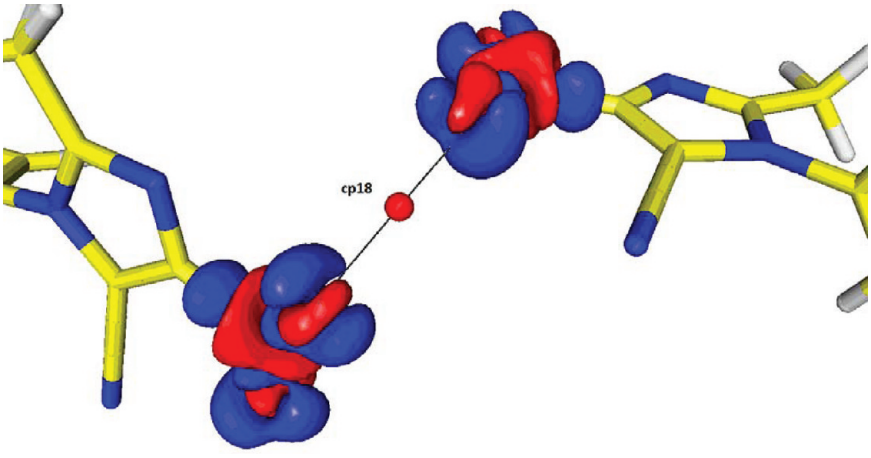

Figure 13. 3D view of the static deformation charge density distribution of two nitro groups in the O···O contact. The CP and bond path are shown.

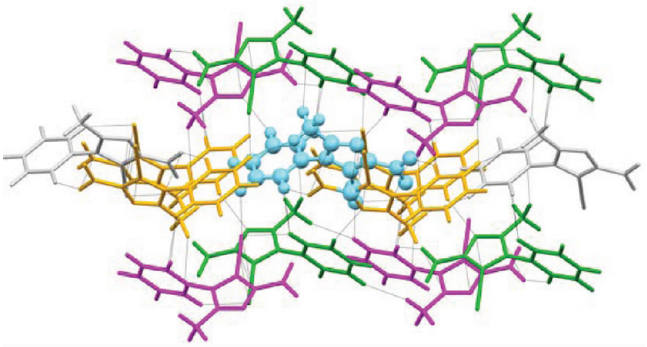

Figure 15. Molecule **1** surrounded by 14 symmetry related molecules (symmetry codes are in Table 7).

Table 7. Electrostatic Interaction Energy (kcal/mol) for Nine Independent Dimers Formed by the Asymmetric Unit and Symmetry Generated Molecules[a]

no.	symmetry code	main interactions	without R_{free} restraints	R_{free}
1	$-x+1, -y, -z+2$*	O81···H2	−18.3	−19.8
		O82···C71		
		C8···N2		
		C7···O81		
2	$-x+2, -y, -z+2$*	N91···H6	−12.9	−19.3
		C5···O82		
		CN···CN		
3	$-x+1, -y, -z+1$*	C2···H3	−24.3	−21.1
4	$-x+2, -y, -z+1$*	H4···H5	−4.6	−5.8
5	$x+3/2, -y+3/2, z+1/2$	H5···N2	−0.89	−0.93
		H5···O81		
6	$-x+3/2, y-1/2, -z+3/2$	C5···H71	−29.1	−27.0
		N91···H71		
		H2···H6		
		C3···C7		
7	$x+1/2, -y+1/2, z+1/2$	H3···N91	−1.6	−1.8
8	$x, y, z-1$	H4···O81	−14.2	−14.6
9	$-x+3/2, y+1/2, -z+5/2$	O81···O82	−10.9	−11.5

[a] Involutional symmetry operators ($\sigma = \sigma^{-1}$) are marked by an asterisk (*). Two molecular models were used: Free and R_{free}.

O···O Contact. Careful analysis of the experimental electron density topology reveals a very weak O···O contact, longer than the sum van der Waals radius (3.47 Å). The angles formed by N−O···N are 145° and 117° (cf. Figure 13). The static deformation density (Figure 14) shows that the O82 electron lone pair of one molecule is directed toward an electron depleted region of atom O81 of the second molecule, so the interaction between the two oxygen atoms is actually not as repulsive as could be expected. Accordingly this interaction is characterized by cp18 and its related bond path (Figures 13 and 14). Such an interaction is similar in nature to that observed for Cl···Cl interactions in hexachlorobenzene.[79] The corresponding electrostatic energy calculated with VMoPro[1−3] for the dimer composed of the two connected molecules is about −11 kcal/mol.

Experimental Electrostatic Energy. There are 14 symmetry related molecules surrounding the 2-methyl-4-nitro-1-phenyl-1*H*-imidazole-5-carbonitryle molecule in the crystal (Figure 15). Among these 14 occurring dimers, nine are independent. The electrostatic energy was calculated with VMoPro[1−3] (Table 7) for each dimer interaction using the R_{free} and Free models. In general, values of the electrostatic energies for these two models differ by less than 8% with the exception for symmetry related molecules #2, #4, and #7, where the changes are 33, 21, and 12%, respectively (Table 7). The highest difference is attributed to the dimer connected via dipole−dipole interaction (no. 2), in line with the changes in Laplacian and λ_3 mentioned before.

These energy calculations clearly address the importance of the multipole refinement strategy and the need to have statistical indices like R_{free} to validate fine refinement details: the experimental electrostatic energy differs by 6 kcal/mol calculated from the Free model (−13 kcal/mol) or the R_{free} strategy (−19 kcal/mol). On the other hand our best theoretical approximation (SCS-RI-MP2-F12) of the total interaction energy is close to −13 kcal/mol, including repulsion and dispersion terms. Therefore one expects the theoretical electrostatic term to be close to that found by our R_{free} model. It is however necessary to systematize how very subtle details may largely affect quantitative electrostatic properties. It can be of utmost importance when applied to protein−ligand interactions for which larger uncertainty of atomic positions will additionally affect the resulting energy.[80]

■ ASSOCIATED CONTENT

Supporting Information. A figure of the static deformation density and tables of bond critical points, selected critical points for **1** and **2**, and topology of intermolecular contacts. This material is available free of charge via the Internet at http://pubs.acs.org.

■ AUTHOR INFORMATION

Corresponding Author

*Email: mkubicki@amu.edu.pl, claude.lecomte@crm2.uhp-nancy.fr.

■ ACKNOWLEDGMENT

This work was partially financed by the grant of Polish Ministry of Science and Education No. N N204 028138 and the French Embassy in Warsaw within the frame of cotutelle bursary for AP. We also thank Université Henri Poincare in Nancy and CNRS for support. We thank Konstantinos Vogiatzis for a helpful discussion.

■ REFERENCES

(1) Guillot, B.; Viry, L.; Guillot, R.; Lecomte, C.; Jelsch, C. *J. Appl. Crystallogr.* **2001**, *34*, 214–223.

(2) Jelsch, C.; Guillot, B.; Lagoutte, A.; Lecomte, C. *J. Appl. Crystallogr.* **2005**, *38*, 38–54.

(3) MoProViewer: a Molecular Viewer Dedicated to Charge Density Analysis. Poster presented at the French Crystallogr. Assoc. AFC2010 (Strasbourg). 7−10 July 2010. http://www.crm2.uhp-nancy.fr/crm2/fr/labo/equipes/emqc/.

(4) Volkov, A.; Macchi, P.; Farrugia, L. J.; Gatti, C.; Mallinson, P.; Richter, T.; Koritsanszky, T. *A Computer Program Package for Multipole Refinement, Topological Analysis of Charge Densities and Evaluation of Intermolecular Energies from Experimental and Theoretical Structure Factors*, 2006.

(5) Bader, R. F. W. *Atoms in Molecules—A Quantum Theory*; Oxford University Press: Oxford, 1990.
(6) Hirshfeld, F. L.; Hope, H. *Acta Crystallogr., Sect. B* **1980**, *36*, 406–415.
(7) Eisenstein, M.; Hirshfeld, F. L. *Chem. Phys.* **1979**, *38*, 1–10.
(8) Sørensen, H. O.; Stewart, R. F.; McIntyre, G. J.; Larsen, S. *Acta Crystallogr., Sect. A* **2003**, *59*, 540–550.
(9) Parfonry, A.; Declercq, J. P.; Tinant, B.; van Meerssche, M. *Acta Crystallogr., Sect. B* **1988**, *44*, 435–440.
(10) Declercq, J. P.; Tinant, B.; Parfonry, A.; van Meerssche, M. *Acta Crystallogr., Sect. C* **1983**, *39*, 1401–1405.
(11) Milián, B.; Pou-Amérigo, R.; Viruela, R.; Ortí, E. *Chem. Phys. Lett.* **2003**, *375*, 376–382.
(12) Hibbs, D. E.; Overgaard, J.; Platts, J. A.; Waller, M. P.; Hursthouse, M. B. *J.Phys.Chem. B* **2004**, *108*, 3663–3672.
(13) Lee, C.-S.; Hwang, T.-S.; Wang, Y.; Peng, S.-M.; Hwang, C.-S. *J. Phys. Chem.* **1996**, *100*, 1934–2941.
(14) Kožišek, J.; Hansen, N. K.; Fuess, H. *Acta Crystallogr., Sect. B* **2002**, *58*, 463–470.
(15) Munshi, P.; Cameron, E.; Guru Row, T. N.; Ferrara, J. D.; Cameron, T. S. *J. Phys. Chem. A* **2007**, *111*, 7888–7897.
(16) Bats, J. W.; Coppens, P.; Kvick, Å. *Acta Crystallogr., Sect. B* **1977**, *33*, 1534–1542.
(17) Bats, J. W.; Coppens, P. *Acta Crystallogr., Sect. B* **1977**, *33*, 1542–1548.
(18) Gopalan, R. S.; Kulkarni, R. U.; Ravi, M.; Rao, C. N. R. *New J. Chem.* **2001**, *25*, 1108–1110.
(19) Gopalan, R. S.; Kulkarni, R. U.; Rao, C. N. R. *Chem. Phys. Chem.* **2000**, *1*, 127–135.
(20) Allen, F. H. *Acta Crystallogr., Sect. B* **2002**, *58*, 380–388.
(21) Paulini, R.; Muller, K.; Diederich, F. *Angew. Chem., Int. Ed.* **2005**, *44*, 1788–1805.
(22) Wood, P. A.; Borwick, S. J.; Watkin, D. J.; Motherwell, W. D. S.; Allen, F. H. *Acta Crystallogr., Sect. B* **2008**, *64*, 393–396.
(23) Lee, S.; Malik, A. B.; Fredrickson, D. C. *Cryst. Growth Des.* **2004**, *4*, 279–290.
(24) Kubicki, M. *Acta Crystallogr., Sect. C* **2004**, *60*, o255–o257.
(25) Paul, A.; Kubicki, M.; Jelsch, C.; Durand, P.; Lecomte, C. *Acta Crystallogr., Sect. B* **2011**, *67*, 365–378.
(26) Kubicki, M.; Borowiak, T.; Dutkiewicz, G.; Souhassou, M.; Jelsch, C.; Lecomte, C. *J. Phys. Chem. B* **2002**, *106*, 3706–3714.
(27) *CrysAlis PRO, (Version 1,171,33,36d)*, Oxford Diffraction Ltd., 2009
(28) Clark, R. C.; Reid, J. S. *Acta Crystallogr., Sect. A* **1995**, *51*, 887–897.
(29) Blessing, R. H. *Crystallogr. Rev.* **1987**, *1*, 3–58.
(30) Altomare, A.; Cascarano, G; Giacovazzo, C.; Guagliardi, A. *J. Appl. Crystallogr.* **1993**, *26*, 343–350.
(31) Sheldrick, G. M., *Institüt für Anorganische Chemie der Universität, Tammanstrasse 4, D-3400 Göttingen*, Germany, 1998.
(32) Madsen, A. Ø. *J. Appl. Crystallogr.* **2006**, *39*, 757–758SHADE web server for estimation of hydrogen anisotropic displacement parameters.
(33) Hansen, N. K.; Coppens, P. *Acta Crystallogr., Sect. A* **1978**, *34*, 909–921.
(34) Clementi, E.; Roetti, C. *At. Data Nucl. Data Tables* **1974**, *14*, 177–478.
(35) *International Tables for Crystallography*; Wilson, A. J. C., Ed.; Kluwer Academic Publishers: Boston, 1992; Vol. C, p 219.
(36) Allen, F. H.; Watson, D. G.; Brammer, L.; Orpen, A. G.; Taylor, R. *International Tables for Crystallography*; Kluwer Academic Publishers: Boston, 2006; Vol. C, Chapter 9.5, pp 790−811.
(37) Domagała, S.; Jelsch, C. *J. Appl. Crystallogr.* **2008**, *41*, 1140–1149.
(38) Brünger, A. T. *Nature (London)* **1992**, *355*, 472–474.
(39) Hirshfeld, F. L. *Acta Crystallogr., Sect. A* **1976**, *32*, 239.
(40) Stash, A; Tsirelson, V. *J. Appl. Crystallogr.* **2002**, *35*, 371–373.
(41) Dirac, P. A. M. *Proc. R. Soc. London, Ser. A* **1929**, *123*, 714–733.
(42) Slater, J. C. *Phys. Rev.* **1951**, *81*, 385–390.
(43) Vosko, S. H.; Wilk, L.; Nusair, M. *Can. J. Phys.* **1980**, *58*, 1200–1211.
(44) Becke, A. D. *Phys. Rev. A* **1988**, *38*, 3098–3100.
(45) Perdew, J. P. *Phys. Rev. B* **1986**, *33*, 8822–8824.
(46) Lee, C.; Yang, W.; Parr, R. G. *Phys. Rev. B* **1988**, *37*, 785–789.
(47) Becke, A. D. *J. Chem. Phys.* **1993**, *98*, 5648–5652.
(48) Hellweg, A.; Hättig, C.; Höfener, S.; Klopper, W. *Theor. Chem. Acc.* **2007**, *117*, 587–597.
(49) Weigend, F.; Häser, M.; Patzelt, H.; Ahlrichs, R. *Chem. Phys. Lett.* **1998**, *294*, 143–152.
(50) Grimme, S. J. *Comput. Chem.* **2004**, *25*, 1463–1473.
(51) Grimme, S. J. *Comput. Chem.* **2006**, *27*, 1787–1799.
(52) Grimme, S. J. *Comput. Chem.* **2006**, *27*, 1787–1799.
(53) Boys, S. F.; Bernardi, F. *Mol. Phys.* **1970**, *19*, 553–566.
(54) Eichkorn, K.; Treutler, O.; Ohm, H.; Häser, M.; Ahlrichs, R. *Chem. Phys. Lett.* **1995**, *240*, 283–289.
(55) Sierka, M.; Hogekamp, A.; Ahlrichs, R. *J. Chem. Phys.* **2003**, *118*, 9136–9148.
(56) Møller, C.; Plesset, M. S. *Phys. Rev.* **1934**, *46*, 618–622.
(57) Klopper, W.; Manby, F. R.; Ten-no, S.; Valeev, E. F. *Int. Rev. Phys. Chem.* **2006**, *25*, 427–468.
(58) Grimme, S. J. *J. Chem. Phys.* **2003**, *118*, 9095–9102.
(59) Peterson, K. A.; Adler, T. B.; Werner, H.-J. *J. Chem. Phys.* **2008**, *128*, 84102.
(60) Yousaf, K. E.; Peterson, K. A. *J. Chem. Phys.* **2008**, *129*, 184108.
(61) Hättig, C. *Phys. Chem. Chem. Phys.* **2005**, *7*, 59–66.
(62) Weigand, F.; Köhn, M.; Hättig, C. *J. Chem. Phys.* **2002**, *116*, 3175–3183.
(63) *TURBOMOLE V6.2* (a development of University of Karlsruhe and Forschungszentrum Karlsruhe GmbH, 1989−2007, and TURBOMOLE GmbH, since 2007. Available from http://www.turbomole.com, 2010.
(64) Fournier, B.; Bendeif, E.-E.; Guillot, B.; Podjarny, A.; Lecomte, C.; Jelsch, C. *J. Am. Chem. Soc.* **2009**, *131*, 10929–10941.
(65) Koritsanszky, T.; Coppens, P. *Chem. Rev.* **2001**, *101*, 1583–1627.
(66) Coppens, P.; Guru Row, T. N.; Leung, P.; Stevens, E. D.; Becker, P. J.; Yang, Y. W. *Acta Crystallogr., Sect. A* **1979**, *35*, 63–72.
(67) Mulliken, R. S. *J. Chem. Phys.* **1955**, *23*, 1833–1831.
(68) Klamt, A.; Schüürmann *J. Chem. Soc., Perkin Trans.* **1993**, *2*, 799–805.
(69) Spackman, M. A.; Munshi, P.; Dittrich, B. *ChemPhysChem.* **2007**, *8*, 2051–2063.
(70) Spackman, M. A. *Chem. Rev.* **1992**, *92*, 1769–1797.
(71) Abramov, Y. A.; Volkov, A. V.; Coppens, P. *Chem. Phys. Lett.* **1999**, *311*, 81–86.
(72) Hao, X.; Chen, J.; Cammers, A.; Parkin, S.; Broc, C. P. *Acta Crystallogr., Sect. B* **2005**, *61*, 218–226.
(73) Ziao, N.; Graton, J.; Laurence, C.; LeQuestel, J.-Y. *Acta Crystallogr., Sect. B* **2001**, *57*, 850–858.
(74) Koch, U.; Popelier, P. L. A. *J. Chem. Phys.* **1995**, *99*, 9747–9754.
(75) Ay, S.; Ziegert, R. E.; Zhang, H.; Nieger, M.; Rissanen, K.; Fink, K.; Kubas, A.; Gschwind, R. M.; Braäse, S. *J. Am. Chem. Soc.* **2010**, *132*, 12899–12905.
(76) Gerenkamp, M.; Grimme, S. *Chem. Phys. Lett.* **2004**, *392*, 229–235.
(77) Anslyn, E. V.; Dougherty, D. A. *Modern Physical Organic Chemistry*; University Science Books: Sausalito, CA, 2006, ISBN 1-891389-31-9.
(78) NIST Standard Reference Database Number 69, available online at http://webbook.nist.gov/chemistry, accessed 31.03.2011
(79) Bui, T. T. T.; Dahaoui, S.; Lecomte, C.; Desiraju, G. R.; Espinosa, E. *Angew. Chem., Int. Ed.* **2009**, *48*, 3838–3841.
(80) Fournier, B.; Guillot, B.; Jelsch, C.; Lecomte, C. *Acta Crystallogr., Sect. D* **2011**submitted.